Pure appl. geophys. 163 (2006) 1515–1536
0033–4553/06/081515–22
DOI 10.1007/s00024-006-0088-0

Pure and Applied Geophysics

A Study of the Adaptive Method for Decoupling Overlapping Seismic Records

XUANHUI YANG,[1] Yu JEFFREY GU,[2] Ping SHEN,[3] Xiqiang LIU,[4] and ZHIZHEN ZHENG[5]

Abstract—Signal extraction from overlapping seismic records is a common problem in geophysical data analysis. Identification and separation of multiple seismic arrivals, analysis of large earthquakes as multiple point sources, and calculation of the true yield of a large nuclear explosion from interfering small explosion, all hinge on our ability to effectively decouple two interfering wave signals. This paper presents a method for signal separation based on an adaptive filtering technique. We apply a semi-deconvolution algorithm to overlapping explosion records and S/SKS phase groups, and then perform noise reduction and signal decoupling under different *a priori* conditions and assess the stabilities using a variance reduction approach. We demonstrate, through numerical experiments and analysis of seismic station records, that the adaptive method can be both robust and practical for regional and teleseismic applications.

Key words: Seismic records, waveform interference, signal processing, SKS splitting, semi-blind deconvolution, adaptive method.

1. Introduction

A classical problem in geophysical signal processing is the extraction of individual signals from composite or overlapping records. For instance, if a small nuclear explosion takes place prior to a subsequent (delayed by ~100 ms) larger explosion, the interference of multiple sources can significantly distort the far-field waveforms produced by the ground motion and, potentially, reduce the peak amplitude of the second explosion. For this very reason, a modified magnitude scale has to be

[1] Institute of Crustal Dynamics, China Earthquake Administration, Beijing 100085, P.R. China.
E-mail: xhyang@seis.ac.cn
[2] Department of Physics, University of Alberta, Edmonton, AB, T6G2J1, Canada.
E-mail: jgu@phys.ualberta.ca
[3] Institute of Geophysics, China Earthquake Administration, Beijing 100086, P.R. China.
E-mail: pingshen279@163.com
[4] Shandong Provincial Seismological Bureau, Jinan 250014, P.R. China.
E-mail: lxq@eqsd.gov.cn
[5] The Center of Seismic Data and Information, Beijing 100045, P.R. China.
E-mail: zhengzhizhen@hotmail.com

considered (MUELLER and MURPHY, 1971; STUMP *et al.*, 1999; XIE, 2002; PHILLIPS *et al.*, 2004) to counteract common yield-masking procedures. On the other hand, a delay-fired approach can be beneficial to mining engineering and hazard mitigation, as seismic coupling offers an effective means to reduce the overall far-field ground motion (see STUMP *et al.*, 1999). Both test-ban monitoring and mining engineering rely on the reconstruction of overlapping seismic records, a major challenge in geophysical data processing.

Effects associated with the superposition of waves are also commonly observed in the physical process of fault rupturing and thereby influence earthquake signal analysis. For instance, large magnitude earthquakes usually do not result from a simple, isolated fault segment, but from a series of brittle failures occurring on multiple fault segments (BRUNE *et al.*, 1969; KANAMORI and STEWARD, 1978; TSENG and SHI, 1978; KANAMORI, 1994). The mechanically strong heterogeneity of individual segments, commonly referred to as ''asperities'' or ''barriers'', requires sufficient elastic strain energy to overcome and can potentially induce a large earthquake (AKI, 1984; KOSTROV and DAS, 1988; SCHOLZ *et al.*, 1993; LAY and WALLACE, 1995; BOUCHON, 1997). Consequently, the far-field seismic record from a large or intermediate earthquake can be a complex overlapping waveform, superimposed by signals from the individual subevents. A similar convolution problem is also encountered in studies of crust and mantle structure when two seismic phases arrive at similar times. For example, SKS and S arrivals overlap in the epicentral distance range of 80–100° and severely limits the available data to SKS splitting and seismic anisotropy (e.g., SILVER, 1996; GAO *et al.*, 1994; LEVIN *et al.*, 1999; BOKELMAN and SILVER, 2002; LEVIN and PARK, 2002). Hence, to decipher earthquake genesis and crust/mantle seismic structures, it is crucial to be able to differentiate multiple seismic sources and propagation effects responsible for an overlapping record.

In theory, the process of signal separation is relatively straight forward, but in practice it is often a daunting task. First, signals that overlap may have a short time separation between them, possibly on the order of tens to hundreds of milliseconds, making it difficult to perform time-domain analysis. A greater challenge is that overlapped signals often contain multiple wavelets with similar spectral characteristics (e.g., DARGANI-NOUBARY, 1999). Although significant progress has been made in understanding earthquake source physics and crust/mantle dynamics, a systematic solution for signal extraction in the time domain remains elusive.

The problem of overlapping signal separation is closely related to signal reconstruction — a procedure that is deployed in a variety of scientific disciplines and practical applications. In a nutshell, ''signal reconstruction'' aims at recovering the entire signal from parts of the signal that are already known in time and/or spectral domains. By definition, this procedure cannot recover unknown information from partially known parameters without important conditions. In other words, the imposed conditions and known portion of the data must contain the complete

information about the signal, such that the process is distinct from ''recovering'' or ''rebuilding'' information that is not already embedded. The sampling theorem (TRETTER, 1976; ROBINSON and SILVIA, 1978) proves that a continuous signal can be reconstructed through sampled values, assuming the signal is finite-frequency and satisfies the following sampling criteria: (1) the sampling rate is sufficiently high, and (2) the known portions of the signal are precisely the sampled values. Despite substantial progress in the last two decades, the theory regarding signal reconstruction is still under development, particularly involving ''phase compensation'', ''amplitude compensation'', or the mixture of the two. Phase compensation refers to the process of reconstructing the original signal only from its amplitude spectrum, whereas amplitude compensation implies reconstructing the original signal only from it phase spectrum. Most of the existing theories and approaches have significant limitations.

This study uses an adaptive method to extract individual signals from overlapping seismic records. We present time-domain separation curves and demonstrate that our approach is both robust and practical. Results of numerical simulations suggest that the extracted time-domain signal agrees with the actual data, to a variance reduction of 85% or higher. We present both the merits and limitations of our approach through common problems in explosion monitoring and SKS splitting.

2. Theory

To reconstruct a signal we must solve two problems. First, we need to identify the necessary conditions, generally requirements from the laws of physics, such that the entire signal can be determined from parts of the known data field. Second, we need to develop effective algorithms for a computationally inexpensive reconstruction. Because most data contain noise and suffer from inaccuracies, a practical reconstruction algorithm must be sufficiently insensitive to such effects.

The problem of signal reconstruction can generally be regarded as a ''semi-blind deconvolution'' problem. If signal z_n (n is the iteration number) can be represented as the output of an input signal x_n acted upon by an operator (or machine) y_n, then the problem of solving for x_n and y_n knowing z_n (the convolution of the two) is called ''blind deconvolution'' (LI, 1995; CREPE *et al.*, 1999). Normally the solution to this problem is non-unique and the number of solutions is infinite. Beside z_n, if we also have *some* information about x_n and y_n, we can potentially find a unique solution to this deconvolution problem (SAYED, 2003). This conditional approach is often referred to as ''semi-blind deconvolution'', a terminology occasionally encountered in seismic prospecting, image reconstruction, and projection recovery (e.g., MENDEL *et al.*, 1983; YANG *et al.*, 1998, 1999; CICHOCKI and AMARI, 2002). Semi-blind deconvolution problems can be divided into two subsets — linear and nonlinear problems. Linear

problems involve substantial knowledge about the signal under investigation, whereas problems with little knowledge about the signal are generally considered nonlinear. We will be examining the latter in the subsequent sections.

2.1 Adaptive Noise Filter

In signal processing, an adaptive filter is governed by the following iterative relations (e.g., SAYED, 2003),

$$\begin{cases} y_j = W^T X_j \\ e_j = d_j - y_j \\ W_{j+1} = W_j + 2\mu e_j X_j \end{cases}, \tag{1}$$

where μ is a positive real-valued constant, also referred to as the convergence factor. X_j represents the extracted model from the j-th iteration, and y_j (a scalar) represents the predicted model value using vector X_j. We use e_j to represent the scalar residual relative to the observation d_j for iteration j, assuming a filtering factor (or tap-weight vector) of W_j; the superscript T represents the transpose of a matrix or a vector. Finally, W_{j+1} is the updated value of the filtering factor at step $j+1$ and we minimize the residual e_j by iteratively updating X and W.

Our signal extraction algorithm is based on the adaptive noise reduction scheme with two necessary inputs. If we use x_j to represent the original data that contain noise, then $x_j = s_j + v_0(j)$, where s_j is the signal and $v_0(j)$ represents the noise computed for the j-th iteration. We then adopt a known function $v_1(j)$, intrinsically associated with $v_0(j)$, as the "reference input" and use x_j as the "original input". Since the adaptive filter AF is driven by error e_j, we adjust W (filter response) iteratively such that the output y_j from AF (see Fig. 1 for schematic diagram) approaches $v_0(j)$, which means e_j approaches the signal s_j.

To demonstrate the validity of the above procedure, we set the average values of s_j, v_0 and v_1 to 0. From Figure 1 and equation (1), we obtain

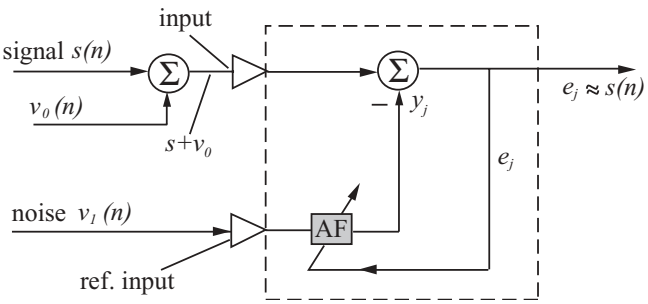

Figure 1
A schematic diagram showing the components and flow of an adaptive noise filter. See section 2 for details.

$$e_j = x_j - y_j = s_j + v_0(j) - y_j \tag{2}$$

$$e_j^2 = s_j^2 + \left(v_0(j) - y_j\right)^2 + 2s_j\left(v_0(j) - y_j\right). \tag{3}$$

Solving for the expected value $E\left[e_j^2\right]$ leads to

$$E\left[e_j^2\right] = E\left[s_j^2\right] + E\left[v_0(j) - y_j\right]^2 + 2E\left[s_j\left(v_0(j) - y_j\right)\right]. \tag{4}$$

We use the process of adaptation to adjust W and minimize $E\left[e^2\right] = \min.$ $E\left[s_j^2\right]$ in equation (4) is not related to W since s_j and $v_0(j)$ are not related to y_j; this implies $E\left[s_j\left(v_0(j) - y_j\right)\right] = 0$. To minimize $E\left[e^2\right]$ we require the second term of equation (4) to be minimized, that is,

$$E\left[v_0(j) - y_j\right]^2 = \min. \tag{5}$$

Because $e_j - s_j = v_0(j) - y_j$, $E\left[e_j - s_j\right]^2$ becomes $E\left[v_0(j) - y_j\right]^2$. Therefore, by minimizing $E\left[e_j - s_j\right]^2$ we obtain both the minimum of $E\left[v_0(j) - y_j\right]^2$ and the lowest variance of $\left(e_j - s_j\right)$. The ideal scenario is

$$\begin{cases} y_j = v_0(j) \\ e_j = s_j \end{cases}. \tag{6}$$

Note that the above proof requires $v_1(j)$ to be, in some way, related to $v_0(j)$ but not s_j. In reality, however, our experiments indicate that desirable separation results can still be achieved when $v_1(j)$ and s_j are weakly coupled. This property makes aforementioned algorithm particularly useful for a wide-range of applications since $v_1(j)$ and s_j are, generally, not independent in most geophysical problems.

3. Numerical Simulation for Separation of Overlapping Signals

As mentioned in Section 1, small explosions are often used 100–200 milliseconds prior to a large explosion to masquerade the peak signal amplitude, hence the true yield of the large explosion. The effective separation of the two overlapped signals requires additional assumptions and constraints, or the solution to the problem would be non-unique. Two key conditions we examine in this study are as follows:

Condition 1: A single explosion previously took place at the same location as the current event and was recorded by the same station. Also, the intensity detailed knowledge about the intensity ratio between the large and small explosions under discussion is known.

Condition 2: A single explosion took place at the same location, recorded by the same station, and that the first arriving phase reflects that of the isolated waveform of the small explosion (i.e., without significant interference with that of the larger explosion).

3.1. Simulation Under Condition 1

Figure 2A shows the unfiltered waveform of an industrial explosion, sampled at 100 Hz. We normalize the intensity by 1/2, and then shift the waveform by 200 milliseconds (20 time samples) to an earlier time (Fig. 2B). Figure 2C shows the sum of the original and modified traces, the synthesized overlapping signal. By default, the superimposed signal 2C undergoes waveform distortion and amplitude reduction with respect to the original record.

The next task is to solve the delay time and recover the two overlapping signals 2A and 2B. We multiply trace 2A by a factor z (where $z \ll 1$) and use the scaled trace as the reference input; the scaled A is effectively the clean, single-explosion source needed for the adaptive filter. During the filtering process we adjust two parameters — the delay time t and reference input amplitude factor z. Incorrect delay times and errors in the amplitude factor z can cause inaccuracies in the final solution. We adopt a trial-and-error solution to the iterative formulation below,

$$\begin{cases} y_j = W^T X_j(i+t) \cdot z \\ e_j = d_j - W^T X_j(i+t) \cdot z \end{cases}, \tag{7}$$

where X_j and d_j are the traces shown in Figures 2A and 2C, respectively. We take time delay of $t = 5, 10, 15, 20, 25, 30$ samples, and for each t compute e_j using $z = 0.06, 0.07, \ldots, 0.20$. The total number of solutions is 90 and each solution contains two traces, one for the large explosion and one for the time-shifted small explosion. We compare the solution with the original, unmodified traces by calculating for each pair of solution traces we calculate the ratio of their peak amplitudes (Ae/Ar), where Ae and Ar are the peak amplitudes of the large and small explosions, respectively. Table 1 shows a subset of the (t, z) pairs and the corresponding ratios for candidate solutions; the best candidate pairs are highlighted.

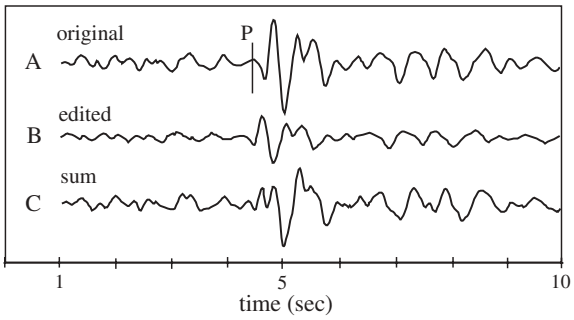

Figure 2
Waveforms of the original and simulated overlapping signal. Trace A is the original signal; trace B a synthetic signal obtained by normalizing the intensity of trace A by 1/2 and shifting A by 200 ms. Trace C is A + B and represents a synthetic overlapping signal.

Table 1

Condition 1 separation result. The time shift is represented by tand the amplitude ratio of the large explosion and the small explosion is represented by z. Potential candidates are in bold letters

t / *z*	5	10	15	20	25	30
0.08	2.405	2.622	2.929	3.274	3.399	3.115
0.09	2.143	2.328	2.616	2.967	3.088	2.813
0.10	**1.933**	2.113	2.366	2.722	2.840	2.572
0.11	1.761	**1.938**	2.162	2.521	2.637	2.375
0.12	1.618	1.792	**1.993**	2.353	2.468	2.210
0.13	1.502	1.668	1.852	2.211	2.324	2.071
0.14	1.403	1.562	1.703	2.090	2.202	**1.952**
0.15	1.318	1.470	1.625	**1.985**	2.095	1.849
0.16	1.242	1.390	1.556	1.897	**2.002**	1.758
0.17	1.176	1.319	1.521	1.819	1.920	1.678
0.18	1.117	1.256	1.490	1.749	1.847	1.607

From Table 1 we find that the two separated signals have peak amplitude ratios close to 2.0, the ideal value, when (z, t) is (5, 0.10), (10, 0.11), (15, 0.12), (20, 0.15), (25, 0.16) or (30, 0.14). To select the optimal result out of these six (z, t) pairs, we compute the mean square deviation between each pair of extracted large (*ext*) and small (*rema*) explosions, that is,

$$EE = \frac{1}{N}\sum_{i=1}^{N}[ext(i+t) - 2 \times rema(i)]^2. \tag{8}$$

In the above equation, t is the delay time expressed in time samples, "2" in the square bracket is the scaling factor, and N is the total number of time samples in the time series (i.e., signal length). The optimal value of z is 0.15 and different values of t are tabulated in Table 2. When $t = 20$ and $z = 0.15$, the mean square deviation 0.252 is the significantly smaller than other values; we thereby determine (20, 0.15) to be the optimal choice of signal separation parameters.

Figure 3 shows the input reference trace (3A), the trace to be extracted (3B), the final extracted signal (3C, the large explosion), the simulated overlapped signal (3D) and finally, the residual trace after extraction (3E, the small explosion). The excellent agreement between 3B and 3C clearly reflects the success of our adaptive procedure. The final simulated signal D nearly reproduces the input overlapping signal shown in

Table 2

Mean-squared deviations for the case of z = 0.15 under condition 1. The optimal solution is in bold letters

T	5	10	15	**20**	25	30
EE	1.087	1.051	1.318	**0.252**	2.218	1.642

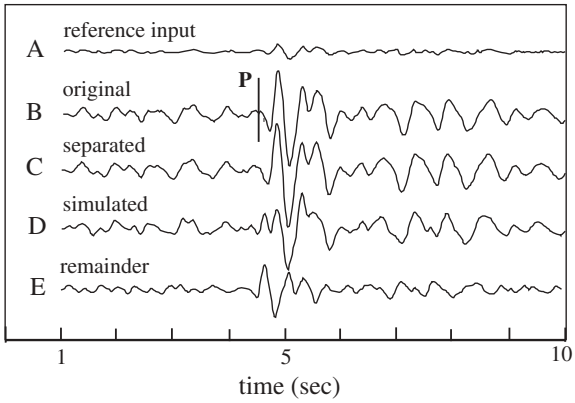

Figure 3
Results of separation for the simulated overlapping signal. A is reference input, B is original signal, C is the separated waveform for B, D is simulated waveform for the overlapping signal (see Figure 2C), and E is remainder. The result of separation is clearly demonstrated by the excellent agreement between the original signal B and the separated result C.

Figure 2C, and the remainder compares well with the targeted small explosion shown by Figure 2B.

In short, the above adaptive deconvolution approach involves (1) using the record of a past single explosion as the input parameter, (2) filtering based on a series of delay time and scaling factor pairs (t, z), (3) finding the pool of solutions that produces the ratios of peak signal magnitudes close to an expected value and, finally, (4) computing the mean square deviation of each pair of resulting signals from the traces. The optimal solution is the one with the smallest deviation.

3.2. Simulation Under Condition 2

In this experiment we again use the model traces shown in Figure 2, but impose a condition that the first peak of the overlapping signal be the original waveform of the smaller explosion. This condition is more practical than condition 1 since we generally have little knowledge about the intensity contrast between the major and minor explosions. We start with the same process as in case 1 where separation is performed under different (t, z) values, but this time we do not compute the ratio of the peak amplitudes of the resulting signals. Instead, we determine the amplitude ratio between the first peak of the remaining signal *rema* (the time-shifted small explosion) and that of the mixed trace (*mix*), that is,

$$mr = mix(1)/rema(1). \tag{9}$$

This procedure produces 90 *mr* ratios and the best 35 are shown in Table 3. The values of *mr* are close to 1.0 when (t, z) is equal to (5, 0.14), (10, 0.14), (15, 0.14), (20,

Table 3

First arrival amplitude ratio z (under condition 2) of the remaining signal rema and the mixed trace mix. Time delay is represented by t. The best candidates are bold

t / *z*	5	10	15	20	25
0.10	1.415	1.417	1.381	1.280	1.415
0.11	1.286	1.286	1.164	1.390	1.192
0.12	1.179	1.279	1.067	1.067	1.179
0.13	1.187	1.090	1.062	**0.985**	1.088
0.14	**1.010**	**1.012**	**1.012**	0.914	**1.010**
0.15	0.943	0.943	0.921	0.853	0.943
0.16	0.884	0.886	0.800	0.955	0.884

0.13) and (25, 0.14). To select the best result out of these five candidates we compute the variance of the difference (*msd*) between the two signals,

$$msd = \frac{1}{N}\sum_{i=1}^{N}[ext(i+t) - z \times rema(i)]^2, \tag{10}$$

where *ext* represents the edited large explosion signal and z is the amplitude ratio taking on possible values of 0.1, 0.2, …, 1.0, 1.1, …, 3.0. The value of t represents the time difference between the two separated signals.

Figure 4 shows the *msd* curves for $t = 5$, 10, 15, 20 and 25. The only curve that has a local minimum (derivative = 0) is when $t = 20$, which strongly suggests that (20, 0.13) is the optimal separation result. The resulting seismograms (Figure 5) show a peak amplitude ratio of 2.05, close to the ideal value of 2.0, and the time delay between the traces is $t = 20$ sample points. The success of the extraction procedure is evidenced by the high correlation between the extracted large explosion signal C and the waveform of the starting signal B.

The above algorithm applies the adaptive filter under the assumption that a pre-existing single (isolated) explosion record can be used as the reference input. The process can be summarized by four steps, namely (1) extract the signals under different delay time t and amplitude factors z through trial and error, (2) find the candidate solutions (t, z) with amplitude ratios between the first peak of the overlapping signal and the residual signal close to 1, (3) solve the variance for each candidate *msd*, and (4) select the optimal solution that contains a local minimum.

3.3. Separation of Signals Produced by Different Source Mechanisms

Earthquake signals present a greater challenge than the two cases examined in the previous section due to variations in source mechanisms. In this section we examine such a hypothetical case with a pair of small (event 1) and large (event 2)

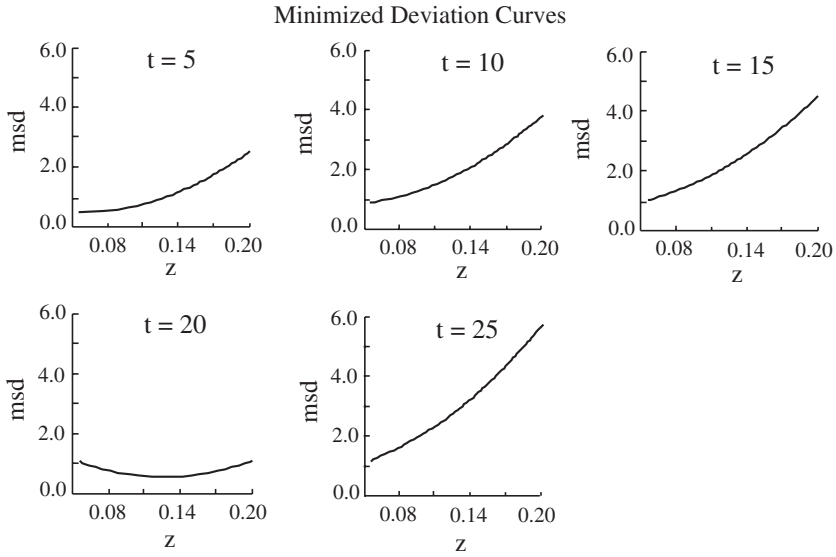

Figure 4
Minimized deviation curves of separated results at $t = 5,10,15,20,25$. The best result is obtained by $t = 20$ where a local minimum (derivative = 0) is present.

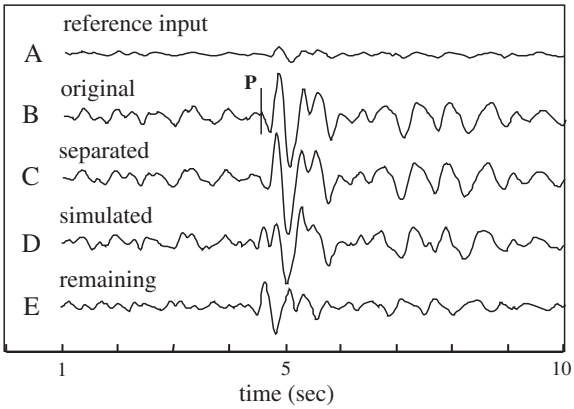

Figure 5
The optimal result of separation ($t = 20$, $z = 0.13$) under condition 2. The trace definitions are the same as Figure 3. We achieve a similar separation result under condition 2 (this figure) as we did under condition 1 (see Figure 3).

earthquakes. To obtain unique and meaningful separation results, we assume a pre-existing event, with a similar location and mechanism as event 1, was recorded at the station (new condition 1). We further assume that event 1 is responsible for the first arrival in the overlapping signal (new condition 2).

To find solution to the above deconvolution problem, we first construct a hypothetical signal that satisfies both new conditions. Traces 6A and 6B (Fig. 6) show the respective waveforms of a small and a large earthquake with different mechanisms. Trace 6C shows the sum of the two after applying a time shift of 200 millisec (equivalent of 20 sampling points).

To extract the earthquake signals we multiply trace A in Figure 6 by a factor $z(z \ll 1)$ as the reference input and use the resulting trace as a proxy of an earlier event with a similar mechanism. This representation is, to a certain extent, similar to analyzing a seismic source using the empirical Green's function approach (HATZEL, 1978; HUTCHINGS and WU, 1990). We then apply the adaptive filter for different (t, z) pairs and compute the amplitude ratio between the remaining signal (*rema*) and the complex signal (*mix*) for the first arrival (see Equation 9).

Our procedure yields amplitude ratios (*mr*) of approximately 1.0 when (t, z) is (15, 0.24), (20, 0.26) and (25, 0.22) (Table 4). Because the remaining waveform is dissimilar to the signal of the large event, it is no longer meaningful to compute the mean-squared deviation between the residual trace and the extracted signal. Instead,

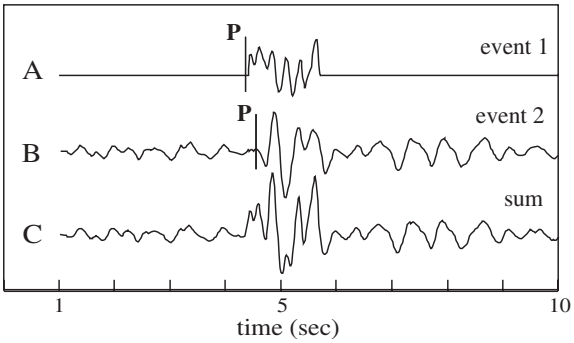

Figure 6
Isolated earthquake signals and synthesized overlapped signal. Trace A is event 1 (see section 3), trace B is a larger earthquake, and trace C represents the sum of the two signals that we use for separation analysis.

Table 4

First arrival amplitude ratio (z) of the remaining signal (rema) and the mixed signal (mix) for earthquake records. The candidate solutions are represented in bold

t / *z*	15	20	25
0.18	1.298	1.397	1.298
0.20	1.168	1.288	1.168
0.22	1.062	1.171	**0.973**
0.24	**0.973**	1.073	0.891
0.26	0.898	**0.967**	0.898

we compute the deviation between the remaining trace (*rema*) and the reference input to rank the three candidates, that is

$$msd = \frac{1}{N}\sum_{i=1}^{N}[rema(i) - z \times input(i+t)]^2. \tag{11}$$

The amplitude ratio z ranges from 0.26 to 0.45, and the delay time t takes on discrete values of 15, 20, and 25 time samples. The mean-squared deviations of the candidate solutions after filtering are shown in Figure 7. The smallest mean-squared deviation 0.136 is obtained by $(t, z) = (20, 0.36)$ (Table 5), which represents the optimal solution to this problem (Fig. 8). As evident in traces shown in 8B and 8C, event 2 record is nearly perfectly recovered after the filtering procedure. Hence, under adequate conditions, one can effectively extract the individual signals from an overlapping signal resulting from two earthquakes of distinct mechanisms.

Still, the experiments of this section show that signal extraction from a convoluted time series is not a simple signal-processing problem. The success of an

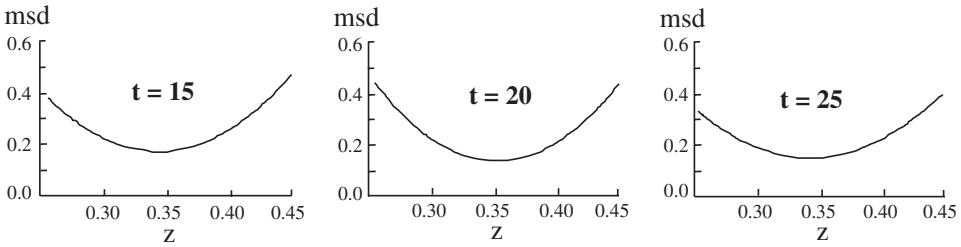

Figure 7
Minimized deviation curves of separated results at $t = 15,20,25$. Each curve contains a local minimum and the optimal solution is determined by the smallest of the three curves (i.e., case $t = 20$).

Table 5

Mean-squared deviation (z) between the remaining and the reference input. Discrete time delays are represented by t

t / *z*	15	20	25
0.32	0.175	0.142	0.147
0.33	0.174	0.139	0.146
0.34	0.174	0.137	0.146
0.35	0.175	**0.136**	0.147
0.36	0.177	**0.136**	0.147
0.37	0.179	0.137	0.151
0.38	0.183	0.139	0.154
0.39	0.187	0.142	0.157
0.40	0.192	0.146	0.161

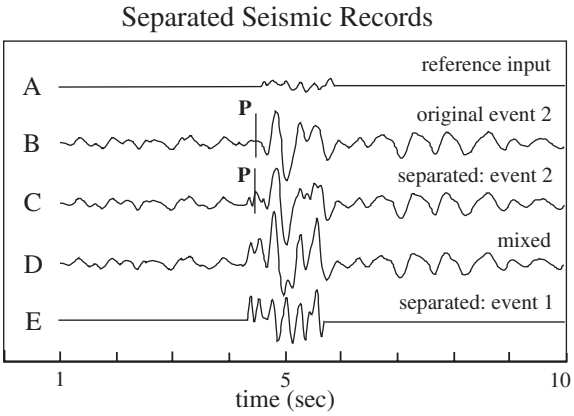

Figure 8
The optimal separation solution for overlapped seismic records produced by different source mechanisms. Trace A is the reference input (event 1), trace B is a larger event (event 2), and trace C is the separated event 2 from the mixed signal. Trace D is the optimal simulated result for the mixed signal and trace E is the separated event 1 record.

algorithm and the choice of input parameters require *some* knowledge about the mechanism(s) that produced the mixed signals. Correct solution can only be achieved when available constraints are effectively applied, and anything less will produce non-unique solutions to the problem.

4. Separation of S and SKS Phases

Seismic anisotropy is a property of rock when its elastic parameters vary as a function of orientation. Its effects are commonly observed in the Earth's mantle and crust, and can cause shear waves to "split" in a fashion similar to birefringence in optics. In recent years, core phases such as SKS have been used extensively in mapping seismic anisotropy in the mantle (e.g., SAVAGE and SILVER, 1993; GAO *et al.*, 1994, 1997; LEVIN *et al.*, 1999; BOKELMAN and SILVER, 2002). Because shear wave loses its "memory" upon converting to P wave within the outer core, the observed splitting can be attributed almost exclusively to the structural properties in the mantle and crust beneath the station. This property makes SKS more desirable than S in imaging mantle anisotropy.

Based on travel time curves, SKS arriving in the epicentral distance range of 80–115° can be utilized for shear-wave splitting analysis. However, the practical distance range is significantly smaller since SKS and S arrivals cross over and interfere at epicentral distances Δ close to 80°. This significantly limits the amount of data available for SKS splitting analysis. Our adaptive method, which can effectively decouple overlapping signals, offers a viable solution to the S-SKS interference

problem. As an example, we apply our method to a $M_b = 6.4$ earthquake occurring on Aug. 5, 1996 in the southern Pacific Ocean. The epicenter location is (20.72 S, 178.29 W) and the focal depth is $h = 531$ km. We use two station records, Qiongzhong (QIZ) and Kunming (KMI), with respective epicentral distances of 80.7° and 89.21° and station azimuths of 294° and 297°.

Figure 9 shows the input waveforms and separation results for two different frequency bands. The two panels starting from left show unfiltered samples taken at respective frequencies of 20 and 1 Hz. In both cases, SKS is fairy isolated at station KMI, but it is overwhelmed by the S arrival at station QIZ. Due to similar azimuths, these two stations can be approximated as being on the same great circle encompassing the earthquake. By this assumption, we use the SKS phase from KMI, time shifted to account for epicentral distance, as the reference input for the adaptive procedure performed on the QIZ records.

To separate S from SKS, the first task is to determine the filtering condition (see section 3) best suited for this problem. According to the definition of body-wave magnitude, the magnitude correction factor $Q(\Delta, h)$ (where Δ is the epicentral distance and h is the earthquake depth) is 0.12 for a 80–90° long , 530-km deep earthquake (Figure 10; SHI *et al.*, 1992). The governing equation is

$$m_b = \log\frac{A}{T} + Q(\Delta, h) + s_i, \tag{12}$$

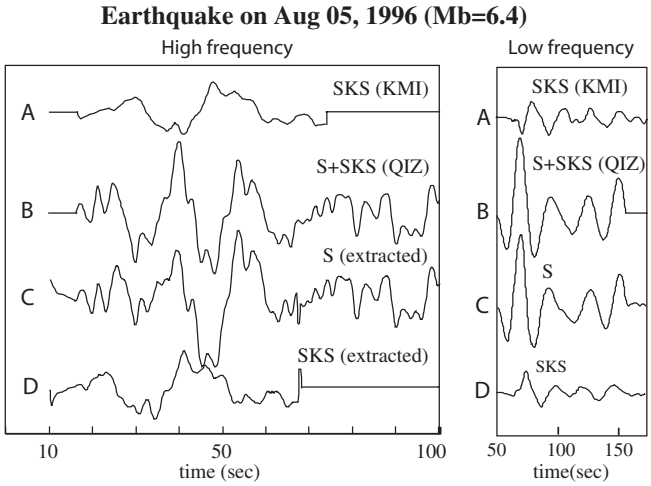

Figure 9

SKS and S + SKS waveforms used in the signal separation. The left and right panels show the respective high-frequency (unfiltered, 20 Hz sampling) and low-frequency (unfiltered, 1 Hz sampling) signals from stations KUM and QIZ. The KMI reference input (A) has been time shifted to correct for epicentral distance and the origin time starts at a selected time window for the S + SKS arrivals.

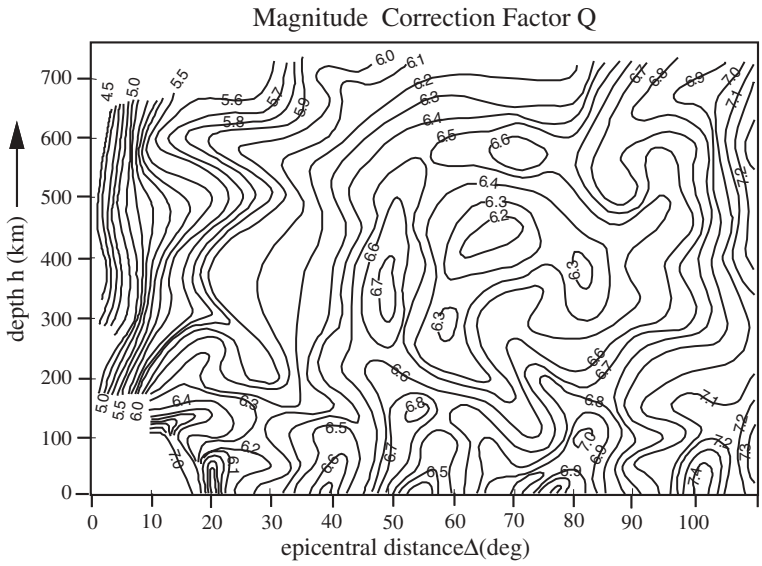

Figure 10
A contour map of Q values for S wave magnitudes. This map is reproduced from SHI *et al.* (1992) based on regional earthquakes in this region. These correction values are used to obtain the optimal SKS amplitude ratio between stations KMI and QIZ.

where A is the maximum horizontal displacement, T is the signal period and s_i is the station correction factor (LAY and WALLACE, 1995). We obtain the S-wave amplitude ratio between QIZ and KMI of 1.31 for the high frequency signal, and adopt this amplitude ratio as condition 1. In other words, the 1.31 amplitude ratio of SKS at these two stations is the adaptation criterion.

For the high frequency signals, we apply the adaptive filtering process for delay times t ranging from 3 to 13 time samples and amplitude factor z ranging from 0.3 to 0.5. The resulting amplitude ratio of SKS arrivals between QIZ (effective remaining signal) and KMI (effective reference signal) is shown in Table 6. Among the 70 entries we obtain 10 candidate solutions with wide-ranging time shifts and z values focused between 0.44 and 0.48. To obtain the best solution from this group we compute the mean-squared deviation between the resulting SKS waveforms from QIZ (*rema*) and KMI (*input*) as follows,

$$EE = \frac{1}{N}\sum_{i=1}^{N}[rema(i) - 1.31 \times input(i+t)]^2, \tag{13}$$

where t is the delay time, and N is the total number of samples. The effective weighted χ^2 criterion (EE) returns the minimum value of 0.232 at $(t, z) = (5, 0.44)$ (Table 7), the optimal solution for the signal separation. The resulting amplitude of the

Table 6

Amplitude ratios of high-frequency solution of M_b = 6.4 earthquake on Aug. 05, 1996

z / *t*	0.30	0.40	0.42	0.44	0.46	0.48	0.50
3	0.90	1.19	1.26	**1.30**	1.36	1.40	1.72
4	0.91	1.21	1.27	**1.33**	1.38	1.44	1.49
5	0.91	1.21	1.27	**1.33**	1.39	1.45	1.46
7	0.90	1.20	1.26	**1.30**	1.36	1.41	1.45
8	0.89	1.18	1.22	**1.28**	1.35	1.40	1.43
9	0.87	1.14	1.21	1.27	**1.34**	1.35	1.40
10	0.88	1.14	1.20	1.25	**1.30**	1.35	1.40
11	0.89	1.15	1.20	1.25	**1.31**	1.35	1.40
12	0.87	1.12	1.20	1.24	1.29	**1.32**	1.40
13	0.87	1.14	1.21	1.26	**1.30**	1.35	1.40

Table 7

The mean squared deviation between the resulting SKS waveform from QIZ (rema) and that from KMI (Ref. input) for the high-frequency recordings, Aug. 05, 1996

t	3	4	**5**	7	8	9	10	11	12	13
EE	0.254	0.240	**0.232**	0.248	0.250	0.256	0.242	0.268	0.258	0.276

reference SKS amplitude at KMI scales to 1.31 with the extracted SKS amplitude at QIZ (see Fig. 9, left). The signals differ significantly in time, but the overall characteristics are fairly consistent, as expected from the same earthquake and largely overlapping great-circle paths.

Assuming the scaling factor is relatively frequency independent, we further examined the low-frequency signals (1 Hz) for the same earthquake. Among the 65 entries tabulated in Table 8, the ratios of five (z, t) pairs are close 1.31 at (20, 0.10), (15, 0.07), (10, 0.04), (5, 0.02), and (0, 0.03). The result of the squared deviation (Table 9) indicates that (t, z) = (10, 0.04) leads to the minimum value and, therefore, to the optimal filtering parameters (see Fig. 9, right). Despite a dominating S-phase signal at QIZ, a clean SKS record with the desired amplitude ratio (see trace D) shows an earlier time and somewhat sharper signal with respect to the input reference signal at KMI.

The success of the above approach should not overshadow the complexities in the problem of SKS-S separation analysis. Such complexities are demonstrated in a similar experiment using a 210-km deep, $M_b = 6.3$ earthquake on July 27, 2003. The respective station distances are approximately 90° and 82° to KMI and QIZ, and the signals are sampled at 1 Hz. Based on magnitude correction map shown in Figure 10, the Q-values should be approximately 6.9 and 6.7 for the earthquake depth of 210 km and station distances of 90° and 82°, respectively. The empirical amplitude ratio

Table 8

The maximum SKS amplitude ratio (z) of extracted QIZ record and the original KMI record for the low-frequency recordings, Aug. 05, 1996

t / *z*	20	15	10	5	0
0.01	0.040	0.049	0.095	0.169	0.443
0.02	0.084	0.101	0.352	**1.267**	0.306
0.03	0.153	0.268	0.751	2.443	**1.134**
0.04	0.304	0.537	**1.379**	3.107	1.994
0.05	0.494	0.866	2.006	3.917	2.218
0.06	0.698	1.175	2.537	4.384	2.980
0.07	0.891	**1.410**	3.073	4.606	3.678
0.08	1059	1.579	3.398	4.739	3.966
0.09	1.199	1.695	3.803	4.848	4.203
0.10	**1.314**	1.773	4.151	4.896	4.274
0.11	1.409	1.827	4.246	4.772	4.271
0.12	1.490	1.866	4.425	4.909	4.316
0.13	1.584	1.895	4.811	5.831	4.297

Table 9

Squared deviation between the two SKS recordings (the extracted SKS from QIZ station and that recorded by KMI station) for the low-frequency recordings, Aug. 05, 1996

(*t*, *z*)	20, 0.10	15, 0.07	**10, 0.04**	5, 0.02	0, 0.03
EE	0.174	0.148	**0.045**	0.442	0.853

between these two stations is ~1.58; this value is used as the primary adaptation condition. Figure 11 shows the waveform (from the start of our selected separation time window). The shifted KMI record (to simulate a theoretical arrival at 82°) is used as the reference input. The separation condition here is only marginally successful as the final simulated overlapped signal (trace C, shaded) differs notably from the input overlapping signal (trace B, shaded). The remarkable recovery of the SKS amplitude ratio (optimal result = 1.5) should be considered with caution. After all, some structural effects from the non-interfering portion of the ray paths and uncertainties in earthquake source corrections (see Fig. 10) can significantly affect the amplitude ratio, hence the separation condition. Differences in the input and output S + SKS trace (Fig. 11, traces B and C) could largely be caused by overfitting the *a priori* SKS amplitude ratio. Therefore, extra care has to be taken when deciding the separation conditions.

In short, the adaptive filtering approach can perform reasonably well under the condition that the QIZ and KMI are approximately on the same great circle that passes the earthquake location. But as Figure 11 shows, *a priori* condition has to be used with caution. If a nearby station cannot be found, a theoretical seismogram can be used as the alternative reference input. There are advantages for each choice of the reference

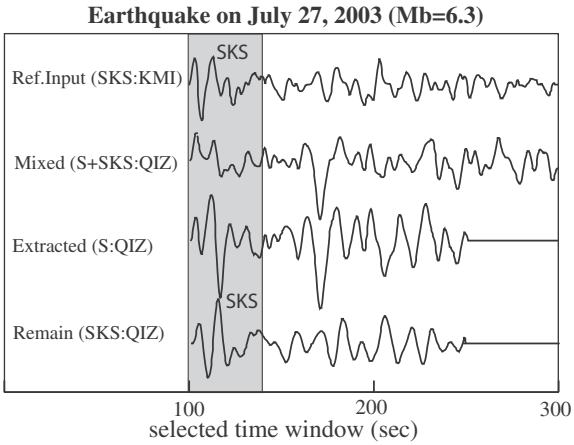

Figure 11
Waveforms and solutions for an $M_b = 6.3$ earthquake on Jul. 27, 2003, similar to Figure 9. The shaded region highlights the S + SKS window. Despite an excellent recovery of the SKS ratio (1.5) in comparison with the *a priori* value (1.58), the notable disagreement between the input (trace B) and simulated (trace C) S + SKS overlapped signal demonstrates the high level of complexity in the signal separation process.

input. For example, it is more *in situ* to use a recorded S or SKS from the same or a nearby station as the reference input, but the requirement is somewhat stringent and high noise level can be inhibitive. On the other hand, synthetic seismograms are noise-free and easy to obtain for a given source-station pair, but they usually differ from actual observations due to effects from, for example, the continental crust. The method of choice is dependent upon the available resources at a given station and the knowledge of the crust and mantle structure beneath a given path.

5. Discussion

We have shown that a modified semi-blind deconvolution method is fully capable of recovering unknown seismic signals from convoluted seismic records. Originating from existing adaptive algorithms frequently encountered in 2-D to 3-D image reconstruction, our approach has significant potentials for the analysis of earthquakes and explosions. This algorithm incorporates techniques known for seismic imaging and verification algorithms (e.g., DARGAHI-NOUBARY, 1999): for example, the use of a characteristic seismic event for signal separation is intrinsically similar to the Empirical Greens Function analysis (HATZEL, 1978; HUTCHINGS and WU, 1990; BERTERO *et al.*, 1998) in strong motion studies and event relocation procedures. For this reason, our adaptive method is only a viable alternative, rather than a replacement, to many of the other signal processing approaches.

The method of choice for effective signal processing strongly depends on the physics of the separation problem and the availability of the seismic phase groups

observed on a given record (SHEARER, 1997; SHEARER and ASTIZ, 1997). For example, improved structural models can be used in concert to improve the waveform and/or travel-time analysis (e.g., ENGDAHL *et al.*, 1998; FLANAGAN and MYERS, 2004). In many cases, the availability of distinctive source spectral and temporal contents is sufficient to infer source characteristics and attenuation (GUPTA *et al.*, 1997; XIE, 2002). For instance, XIE (2002) uses Pn and Lg spectra to discriminate between nuclear and chemical explosions and effectively extract seismic moments (M_0), corner frequencies and Q. Other researchers have applied a simple deconvolution approach based on a characteristic earthquake/explosion taken place at the study region at an earlier time (e.g., HUTCHINGS and WU, 1990; BERTERO *et al.*, 1998). While the success of our adaptive method still impinges on the choices of relatively clean records, the built-in iterative process can sufficiently suppress noise levels and achieve superior signal separation result under appropriate conditions.

In the case of S/SKS separations, our algorithm requires a characteristic earthquake or an in-situ theoretical representation of the Greens function. The determination of a characteristic earthquake requires specific knowledge about a given fault and the stress conditions surrounding the fault. Even more *a priori* information about the explosion records is needed for the synthetic Greens function since it relies on the knowledge of the fault region as well as the structure beneath the source- receiver path. While these are clearly limiting factors for the application of our method, the availability of repeating earthquakes (e.g., ENGDAHL *et al.*, 1998; WALDHAUSER and ELLSWORTH, 2000) ensures that a large fraction of S and SKS overlaps can be removed effectively. Furthermore, with increasing resolution presented by global seismic tomography (DZIEWONSKI and WOODHOUSE, 1987), the details of the mantle structures have also become increasingly clear (e.g., SU *et al.*, 1994; GRAND *et al.*, 1997; VAN DER HILST and KARÁSON, 1999; BOSCHI and DZIEWONSKI, 2001; GU *et al.*, 2001, 2003). The improved knowledge of the basic structure and tectonic history enables more accurate computation of theoretical Greens functions, hence, more accurate filtering result and wider range of applications.

The requisite conditions (or restrictions from the laws of physics) for recovering the entire signal from its parts make our approach "semi-blind". Physically, these requirements show that information is, after all, conserved throughout the signal reconstruction process. Overall, our adaptive method offers a relatively simple time-domain approach that minimizes an objective function. In view of the greater emphasis on seismic anisotropy in recent years, the adaptive method presented by this study can significantly enrich the database for shear-wave splitting measurements by extending epicentral distances close to 80°. While this is only a pilot study aimed at examining the feasibility of the approach, efforts have been undertaken to automate the procedure for large number of seismic records. Because of the simplicity of the adaptive method, a systematic, speedy determination of explosion yield and individual seismic signals is potentially achievable in the near future.

6. Conclusions

This is a pilot study that proposes an adaptive filtering technique to effectively separate two overlapping signals. The main objective is to explore potential seismic applications where the adaptive filtering techniques can be effective. Our experiments show that signal separation is not just a problem of mathematical manipulation, but one that requires a good overall understanding of the underlying physical mechanisms. The proposed approach based on the adaptive-filtering approach is, therefore, not a generic solution to signal separation problems but a candidate solution to wide-ranging applications in earthquake physics and explosion engineering. Results of our simulations only highlight a few of the examples and conditions for seismic analyses. With relatively minor modifications, the same adaptive filtering technique could have significant potentials for future S and SKS splitting analysis and many other aspects of geophysics.

Acknowledgements

We thank Yanping Guo for providing all the data records used in this study. We are also grateful to Brian Mitchell and Kelly Liu for careful reviews and speedy handing of this paper. This study is supported by NSERC Discovery Grant #288160 and the Alberta Ingenuity New Faculty Grant.

References

Aki, K. (1984), *Asperities, barriers, characteristic earthquakes and strong motion prediction*, J. Geophys. Res. *89*, 5867–5872.

Bertero, M., Bindi, D., Boccacci, P., Cattaneo, M., Eva, C., and Lanza, V. (1998), *A novel blind-deconvolution method with an application to seismology*, Inverse Problems *14*, 815–833.

Bokelmann, G.H. R., and Silver, P. (2002), *Shear stress at the base of shield lithosphere*, Geophys. Res. Lett. *28*, 659–662.

Boschi, L. and Dziewonski, A.M. (1999), *'High' and 'low' resolution images of the Earth's mantle - Implications of different approaches to tomographic modeling*, J. Geophys. Res. *104*, 25,567–25,594.

Bouchon, M. (1997), *The state of stress on some faults of the San Andreas system as inferred from near-field strong motion data,* J. Geophys. Res.*, 102*, 11731–11744.

Brune, J.N., Henyey, T.L., and Roy, R.F. (1969), *Heat flow, stress, and rate of slip along the San Andreas fault, California*, J. Geophys. Res. *74*, 3821–3827.

Cappe, O., Doucet, A., Moulines, E., and Lavielle, M. (1999), *Simulation-based Maximum-Likelihood Filter Identification*, Signal Processing Vol., 3–25.

Cichocki, A., and Amari, S., *Adaptive blind signal and image processing* (John Wiley & Sons 2002).

Dargahi-Noubary, G.R., *Time series with applications to seismology* (Nova Science Publishers 1999).

Dziewonski, A.M., and Woodhouse, J.H. (1987), *Global images of the Earth's interior*, Science *236*, 37–48.

Engdahl, E.R., van der Hilst, R.D., and Buland, R.P. (1998), *Global teleseismic relocation with improved travel times and procedures for depth determination*, Bull. Seismol. Soc. Am. *88*, 722–743.

FLANAGAN, M.P., and MYERS, S.C. (2004), *Regional travel-time prediction, uncertainty and location improvement*, Seismic Research Review – Trends in Nuclear Explosion Monitoring *26*, 267–276.

GAO, S., DAVIS, P.M., LIU, H., SLACK, P.D., ZORIN, Y.A., MORDVINOVA, V.V., KOZHEVNIKOV, V.M., and MEYER, R.P. (1994), *Seismic anisotropy and mantle flow beneath the Baikao rift zone*, Nature *371*, 149–151.

GAO, S., DAVIS, P.M., LIU, H., SLACK, P.D., RIGOR, A.W., ZORIN, Y.A., MORDVINOVA, V.V., KOZHEVNIKOV, V.M., and LOGATCHEV, N.A. (1997), *SKS splitting beneath continental rift zones*, J. Geophys. Res. *102*, 22,781–22,797.

GRAND, S.P., VAN DER HILST, R.D., and WIDIYANTORO, S. (1997), *Global seismic tomography: A snapshot of convection in the Earth*, GSA Today *7*, 1–7.

GU, Y.J., DZIEWONSKI, A.M., EKSTRÖM, G., and SU, W.-J. (2001), *Models of the mantle shear velocity and discontinuities in the pattern of lateral heterogeneities*, J. Geophys. Res. *106*, 11169–11199.

GU, Y.J., DZIEWONSKI, A.M., and EKSTRÖM, G. (2003), *Simultaneous inversion for mantle shear velocity and topography of transition zone discontinuities*, Geophys. J. Intl. *154*, 559–583.

GUPTA, I., ZHANG, N.T., and WAGNER, R. (1997), *Low frequency Lg from NTS and Kazakh Nuclear Explosions – Observations and Interpretations*, Bull. Seismol. Soc. Am. *87*, 1115–1125.

HARTZELL, S.H. (1978), *Earthquake aftershocks as Green's functions*, Geophys. Res. Lett. *53*, 1425–1436.

HUTCHINGS, L., and WU, F. (1990), *Empirical Green's functions from small earth quakes: A waveform study of locally recorded afterschocks of the 1971 San Fernando earthquake*, J. Geophys. Res. *95*, 1187–1214.

KANAMORI, H. (1994), *Mechanics of earthquakes*, Annu. Rev. Earth Planet. Sci. *22*, 207–237.

KANAMORI, H., and STEWART, G.S. (1978), *Seismological aspects of the Guatemala earthquake of February 4, 1976*, J. Geophys. Res. *83*, 3427–3434.

KOSTROV, B.V. and DAS, S., *Principles of Earthquake Source Mechanics*. Cambridge Monographs on Mechanics and Applied Mathematics (Cambridge University Press 1988).

LAY, T. and WALLACE, T.C., *Modern Global Seismology* (Academic Press 1995).

LEVIN, V., MENKE, W., and PARK, J. (1999), *Shear-wave splitting in Appalachians and Urals: A case for multilayered anisotropy*, J. Geophys. Res. *104*, 17,975–17,994.

LI, T.H. (1995), *Blind deconvolution of linear systems with multilevel non-stationary inputs*, Annals of Statistics *23*, 690–704.

MAGOTRA, N., JIANG, J., HUSH, D., and TAN, L. (1991), *Seismic Phase Detection and Discrimination Using Adaptive Filter Coefficients*, Proc. 25th Asilomar Conference on Signals, Systems, and Computers, 659–662.

MENDEL, J., *Optimal seismic deconvolution* (Academic Press 1983).

MUELLER, R.A. and MURPHY, J.R. (1971), *Seismic characterization of underground nuclear detonations, Part I. Seismic scaling law of underground detonations*, Bull. Seismol. Soc. Am. *61*, 1675–1692.

PHILLIPS, W.S., PATTON, H.J., TAYLOR, S.R., HANS, E.H., and RANDALL, G.E. (2004), *Calibration for coda based magnitude and yield*, Seismic Research Review – Trends in Nuclear Explosion Monitoring *26*, 449–456.

ROBINSON, E.A. and SILVIA, M.T., *Digital processing and time series analysis*, (Holden-Day 1978).

SAVAGE, M. and SILVER, P.G. (1993), *Mantle deformation and tectonics: Constraints from seismic anisotropy in western United States*, Phys. Earth Planet. Int. *78*, 207–227.

SCHOLZ, C.H., DAWERS, N.H., YU, J.-J., ANDERS, M.H., and COWIE, P.A. (1993), *Fault growth and scaling laws: Preliminary results*, J. Geophys. Res. *98*, 21,951–21,961.

SHEARER, P.M. (1997), *Improving local earthquake locations using the L1-norm and waveform cross-correlation: Application to the Whittier Narrows, California, aftershock sequence*, J. Geophys. Res. *102*, 8269–8283.

SHEARER, P.M. and ASTIZ, L. (1997), *Locating nuclear explosions using waveform cross-correlation*, 19th Annual Seismic Res. Symp. on Monitoring a Comprehensive Test Ban Treaty, Proceedings, 301–309.

SHI, Z.L., ZHANG, S.Q., and ZHAO, R.G., *A Handbook for Seismic Work*, (Seismological Press 1992), pp. 92–97.

SILVER, P.G. (1996), *Seismic anisotropy beneath the continents: Probing the depths of geology*, *Annual Rev. Earth Planet. Sci. 24*, 385–432.

STUMP, B.W., PEARSON, D.C., and REINKE, R.E. (1999), *Source comparisons between nuclear and chemical explosions detonated at Rainier Mesa, Nevada Test Site*, Bull. Seismol. Soc. Am. *89*, 409–422.

SU, W.-J., WOODWARD, R.L., and DZIEWONSKI, A.M. (1994), *Degree-12 model of shear velocity heterogeneity in the mantle*, J. Geophys. Res. *99*, 6945–6980.

TRETTER, S.A., *Introduction to Discrete-time Signal Processing* (Wiley 1976).

TSENG, J.S. and SHI, J.S. (1978), *Source multiplicity of the main shock of the Yong Shan-Da Guan Yunnan Earthquake of May 10,1974*, Acta Geophysica Sinica *21*, 160–173.

VAN DER HILST, R. and KARÁSON, H. (1999), *Compositional heterogeneity in the bottom 1000 km of the Earth's mantle: Toward a hybrid convection model*, Science *283*, 578–584.

WALDHAUSER, F. and ELLSWORTH, W.L. (2000), *A double-difference earthquake location algorithm: Method and application to the northern Hayward Fault, California*, Bull. Seismol. Soc. Am. *90*, 1353–1368, DOI: 10.1785/0120000006.

XIE, J. (2002), *Source scaling of Pn, Lg spectra and their ratios from explosions in central Asia: Implications on identification of small seismic events at regional distances*, J. Geophys. Res. *107*, 10.1029/2001JB000509.

YANG, X., SHEN, P., ZHENG, Z., and LIU, X. (1998), *Adaptive method for separating out shear wave in long-spaced acoustilog data processing*, Oil and Geophysics Prospect *33*, 769–774.

YANG, X., SHEN, P., and DONG, T. (1999), *Research on separating Overlapped Explosion Recordings,* Earthquake Research in China *13*, 25–32.

(Received August 17, 2005, accepted February 20, 2006)